Supplemental Material: Superconducting Single-Layer T-Graphene and Novel Synthesis Routes

Qinyan Gu(顾琴燕),[1] Dingyu Xing(邢定钰),[1] and Jian Sun(孙建)[1,*]

[1] *National Laboratory of Solid State Microstructures,*

School of Physics and Collaborative Innovation Center of Advanced Microstructures, Nanjing University, Nanjing 210093

(Dated: August 2, 2019)

Supplemental Discussions

1. Predicted compounds for C-K system

Using the machine learning accelerated crystal structure search method [1], we have found three new stable/metastable candidates of C-K compounds under pressure: the C_4K with $P4/mmm$ structure, the C_3K_4 with $C2/m$ structure, the C_2K_3 with $C2/m$ structure, as shown in Fig. S1(a). Due to the layered feature of C_4K, it is crucial to choose an approprate functional to account the van der Waal interaction. As listed in Table. S1, we compared the calculated lattice constants with the experimental values for Graphite and bcc Potassium. And we can see that the structure parameters optimized from optB88-vdW [2], optPBE-vdW [3], vdW-DF [4, 5] and vdW-DF2 [6] functionals are relatively consistant with the experimental results. On the other hand, the experimental ground state of potassium at ambient pressure is the bcc form, however, in the calculated results from DFT-D2 [7] and DFT-D3 [8] functionals, the fcc form has lower energy than the bcc form, which is contradicted to the reality. Therefore, we adopted optB88-vdW, optPBE-vdW, vdW-DF and vdW-DF2 functionals in our study to check the stability of C_4K. We can see from Fig. 1 in the main text and Fig. S1(b) in the supplementary materials that C_4K can be stable around 11 GPa. The electronic structures of C_4K has been discussed extensively in the main text. And the electronic structure for C_3K_4 and C_2K_3 are shown in Fig. S2. One can find that $C2/m$_C_3K_4 is an insulator with a direct band gap of around 1.45 eV; and $C2/m$_C_2K_3 is metallic. The calculated lattice parameters of all the relevant structures are listed in Table. S2.

*Correspondence should be addressed to J.S. (E-mail:jiansun@nju.edu.cn)

2. The phonon spectra of C-K system

To verify the dynamic stability of C_3K_4, C_2K_3 and C_4K, we calculate the phonon spectra for them. At 20 GPa, C_3K_4 and C_2K_3 are thermodynamically stable and metastable, respectively. As shown in the phonon spectra at corresponding pressure in Fig. S3, there is no imaginary frequency, therefore all the phases are dynamically stable.

3. The effect of the potassium atoms on the exfoliation

The electrochemical method has been used to exfoliate the layered materials. [9–12] As been widely used, we adopted a slab model with vacuum/slab/vacuum geometry to calculated the exfoliation energy of T-graphene from C_4K, as shown in Fig. S4(a). As the topmost T-graphene moving away from the parent compound, we calculated the exfoliation energy with two different methods, one is fully relaxing the remaining potassium atoms and T-graphene layers, and the second one is only relaxing the topmost layer of potassium atoms. As the results shown in Fig. S4(b), the difference between the exfoliation energies from the two methods is small, which indicates that the influence from the relaxation of the potassium atoms is negligible. It has been reported that in some cases, the intercalants can help to lower the exfoliation energy of graphene. [9] However, in our calculations, the presence of potassium atoms layer increases the exfoliation energy of the T-graphene. We calculated the charge transfer of the GICs and C_4K, as shown in Table. S3, the charge tranfer of these materials are very similar. Although these systems do have ionic-like interactions, it has been reported that the graphite intercalation compounds (GICs), such as C_8Li, C_8Na, C_8K and C_6Li are exfoliatable in experiments using electrochemical exfoliation method [13–15]. Therefore, the exfoliation of T-graphene from C_4K using the electrochemical exfoliation method should also be feasible.

4. Potential energy barriers of moving K atoms in C_4K

Duck Young Kim et al. [16] reported the experimental synthesis of a new orthorhombic allotrope of silicon, Si_{24} from a parent compound Na_4Si_{24}. There are some open channals along x axial in Si_{24}, which allow the Na atoms to move, as shown in Fig. S5(c). Along x axis, the stacking sequence of the Na atoms is ABAB... We use a slab model with vacuum/slab/vacuum to calculated the potential energy barrier of moving the Na atom inside the channal of Na_4Si_{24}, as the one Na atom moves through the position along x axis, with the slab of $2 \times 1 \times 1$ and $3 \times 1 \times 1$ cell of the silicon clathrate, as shown in Fig. S5(d). We found the number of layers has very little influence on the calculated potential energy. Fig. S5(a) and (b) depict the route map and potential energy barriers of moving the K atom in

C_4K. Considering the potential energy are mainly from the interaction between the neighboring layer of K atoms and T-graphene, we build the slab of T graphene/K atoms/T graphene with a vacuum layer of 20 Å. We design two directions to move K atom and the potential energy barrier of moveing K atoms in C_4K is slightly lower than that of moving Na atom in Si_{24}, which indicates the feasibility of getting a pure bulk C_4 T-graphene without K atoms by similar procedures from C_4K.

5. The electronic structures for C_4K

In GICs, the interlayer states have a dramatic effect on the electronic structures, so it is important to explore the role of these interlayer states in C_4K. We calculated the band structures of an empty C_4 layer without potassium atoms (C_4K_0), which is obtained by removing the K atoms from the C_4K structure and holding the same lattice constants at 0 GPa without geometry optimization. As shown in Fig. S6, the bands near the Fermi level are mainly contributed by the p_z orbitals. And the doping atoms almost have no effect on the shape of the electronic dispersion. However, the additional electrons donated from K atoms make the Fermi level in C_4K shift up by around 3.05 eV compared with that in C_4 at 0 GPa, which leads to an increase in the occupancy of the π bands. It is reported that the π bands occupancy is helpful to the emergence of superconductivity in GICs [17]. The interlayer bands originated from the s orbital of K atom acts as the conduction band and is close to the Fermi level. In C_4, the bands crossing the Fermi level form a vase shaped and distorted cylindrical Fermi surfaces along the $A-M$ line (shown in Fig. S6(a)). While in C_4K, only one band crosses the Fermi level and the relatively smooth cylindrical Fermi surface can be seen in Fig. S6(b).

6. the superconductivity in C_4K and T-graphene

The electron-phonon coupling (EPC) constant (λ) can be calculted using $\lambda = \frac{N(0)D^2}{M{\omega_{ph}}^2}$. Here, N(0) is the DOS at the Fermi level, M and ω_{ph} are the effective atomic mass and phonon frequency from different atomic species and phonon vibrations, D represents the deformation potential [18, 19], and $D = \frac{\Delta\varepsilon_k}{\Delta Q}$, where ΔQ is the amplitude of phonon mode and $\Delta\varepsilon_k$ is the shift for state near the Fermi level caused by the strong coupling between the phonon modes and Fermi surface. In T-graphene, the acoustic modes in the low-frequency range ($0 \sim 175\,\mathrm{cm}^{-1}$) are responsible for the majority of the value of λ. Among these three acoustic modes, the softest out-of-plane mode (mode_1) has the largest phonon linewidth, which gives rise to the highest peak in the Eliashberg spectral functions. Although

the phonon linewidth of the high-frequency modes seems to be much larger than that of the low-frequency modes, these high-frequency modes have in-plane vibrations thus they contribute very little to the EPC. To figure out what happened, we choose the optical mode at the X point (B_{3u} mode with $\omega \sim 1400\,\mathrm{cm}^{-1}$) as a sample, shown in Fig. S7(a). In Fig. S7(b), we calculate the band structure of T-graphene under the perturbation from the B_{3u} mode with a value of ΔQ to 0.1 $\mathring{A}$. We can see that the perturbated band has the similar behavior as the unperturbated one. Therefore, the influence on the electrons on the Fermi level from the in-plane vibration of the high-frequency modes is not large.

In Fig. S8, we plot phonon dispersions together with phonon linewidth, Eliashberg spectral function $\alpha^2F(\omega)$, electron-phonon coupling strength $\lambda(\omega)$ and phonon density of states (PHDOS) of T-graphene at ambient pressure. We can see that most contributions for the electron-phonon coupling constant arise from the low-frequency modes, mostly related to the vibration of K atoms and the out-of-plane E_g mode of the carbon sheet. This also corresponds to the two predominant peaks in the Eliashberg spectral functions α^2F at about 300 and 450 cm^{-1}. We also calculate band structures and Fermi surfaces after perturbation along the E_g phonon mode in Fig. S8 (c) and (d) To provide more insights on the electron-phonon coupling. The perturbated interlayer band near Γ point is dramatically lowered with the decreasing occupation of π bands. Particularly, the unperturbated interlayer bands have a gap near the Fermi level around the Γ point while the perturbated bands touch together and bring a new electron pocket at the Γ point. These results clearly show that the low-energy carbon out-of-plane vibrations are critical to the electron-phonon pairing, similar as the case in GICs.

In TGICs, the interlayer band is close to the Fermi level and easy to be effected by the pressure. We therefore calculated the electronic structures of C_4K at different pressures (shown in Fig. S9) to see the effect of pressure. The gap between the conduction band from the interlayer state and the fermi level becomes larger under pressure. The interlayer band would occupy the fermi energy after the perturbation of the E_g phonon mode. From Fig. S9, we can see that this phenomenon is increasingly vague with pressure.

On the basis on BCS theory [20] for conventional superconductivity, the emergence of superconductivity depends on two factors: EPC constant λ and Coulomb repulsion parameter μ. When $\lambda >> \mu$, superconductivity occurs. Among them, the parameters λ and μ satisfy the equations $\lambda = N_F V_{ep}$ and $\mu = N_F V_{ee}$, respectively. N_F is the electron DOS at the Fermi level, V_{ep} is the effective e-ph attractive potential and V_{ee} is the effective e-e repulsive potential. Since parameter μ is insensitive to materials, it is a constant and adjustable in the refined McMillian equation [21]: $T_c = \frac{\omega_{log}}{1.2} \exp\left[-\frac{1.04(1+\lambda)}{(\lambda-\mu^*(1+0.62\lambda))}\right]$. The expression of T_c is also related to the characteristic phonon frequency ω_0. We

list the correlation parameters of C_4K and T-graphene in Table. S4. We can see that the N_F for C_4K almost equals to that for T-graphene because of their similar electronic structures. The V_{ep} of T-graphene is larger than that of C_4K, which indicates that the carbon out-of-plane vibration in T-graphene has stronger response to the electrons than that in C_4K. So the λ in T graphene is larger than that in C_4K. However, in bulk C_4K, the carbon out-of-plane vibration strength is quiet high and leads to a peak of PHDOS. The value of PHDOS in C_4K is an order of magnitude higher than that in T-graphene. As a result, the value of logarithmically averaged phonon frequency ω_{log} in C_4K is almost twice as much as that in T-graphene. In BCS theory, logarithmically averaged phonon frequency ω_{log} is positively correlated to T_c, so C_4K has superior superconducting T_c than that of T-graphene.

It is reported that the pressure is an effective way to raise the superconducting temperature in GICs.[22] We therefore studied the superconducting temperature of C_4K as a function of pressure and the results are shown in Fig. S10(a) and (b). It reveals that the value of T_c in C_4K reduces with pressure. One can note that the calculated T_c follows the trend of λ. We guess the reason is the weakness of the coupling between interlayer states and carbon out-of-plane vibrations. Under pressure, the distance between the intercalant and carbon sheets is reduced and the strong confinement of interlayer state would increase its energy. The deformation potential becomes bigger with pressure due to the increasing sensitivity to the perturbation by interlayer states. But the intercalant band shifts up and its occupation reduces (see Fig. S9), the coupling between the interlayer states and carbon out-of-plane vibrations is therefore weaken. The superconductivity of C_4K would be suppressed when the intercalant band is away from the Fermi level, similar to the situation in bulk LiC_6 [23].

[1] K. Xia, H. Gao, C. Liu, J. Yuan, J. Sun, H.-T. Wang, and D. Xing, Sci. Bull. **63**, 817 (2018).
[2] J. Klimeš, D. R. Bowler, and A. Michaelides, J. Phys.: Cond. Matt. **22**, 022201 (2009).
[3] J. Klimeš, D. R. Bowler, and A. Michaelides, Phys. Rev. B **83**, 195131 (2011).
[4] M. Dion, H. Rydberg, E. Schröder, D. C. Langreth, and B. I. Lundqvist, Phys. Rev. Lett. **92**, 246401 (2004).
[5] G. Román-Pérez and J. M. Soler, Phys. Rev. Lett. **103**, 096102 (2009).
[6] K. Lee, E. D. Murray, L. Kong, B. I. Lundqvist, and D. C. Langreth, Phys. Rev. B **82**, 081101 (2010).
[7] S. Grimme, J. Comput. Chem. **27**, 1787 (2006).
[8] S. Grimme, J. Antony, S. Ehrlich, and H. Krieg, J. Chem. Phys. **132**, 154104 (2010).
[9] G. Yoon, D.-H. Seo, K. Ku, J. Kim, S. Jeon, and K. Kang, Chem. Mater. **27**, 2067 (2015).
[10] A. Ambrosi, Z. Sofer, and M. Pumera, Small (2015).
[11] A. Ambrosi and M. Pumera, Chem. Soc. Rev. (2018).
[12] H.-R. Kim, S.-H. Lee, and K.-H. Lee, Carbon **134**, 431 (2018).
[13] J.-W. Lee, M. Kim, W. Na, S. M. Hong, and C. M. Koo, Carbon **91**, 527 (2015).
[14] G. Bharath, E. Alhseinat, N. Ponpandian, M. A. Khan, M. R. Siddiqui, F. Ahmed, and E. H. Alsharaeh, Separation and Purification Technology **188**, 206 (2017).
[15] D.-G. Thomas, E. Kavak, N. Hashemi, R. Montazami, and N. Hashemi, C **4**, 42 (2018).
[16] D. Y. Kim, S. Stefanoski, O. O. Kurakevych, and T. A. Strobel, Nat. Mater. (2015).
[17] G. Csanyi, P. B. Littlewood, A. H. Nevidomskyy, C. J. Pickard, and B. D. Simons, Nat. Phys. **1**, 42 (2005).
[18] F. S. Khan and P. B. Allen, Phys. Rev. B **29**, 3341 (1984).
[19] J. M. An and W. E. Pickett, Phys. Rev. Lett. **86**, 4366 (2001).
[20] J. Bardeen, L. N. Cooper, and J. R. Schrieffer, Phys. Rev. **108**, 1175 (1957).

[21] P. B. Allen and R. C. Dynes, Phys. Rev. B **12**, 905 (1975).
[22] A. Gauzzi, S. Takashima, N. Takeshita, C. Terakura, H. Takagi, N. Emery, C. Hérold, P. Lagrange, and G. Loupias, Phys. Rev. Lett. **98**, 067002 (2007).
[23] G. Profeta, M. Calandra, and F. Mauri, Nat. Phys. **8**, 131 (2012).

Supplemental Tables and Figures

TABLE S1: The calculated relative error from different vdW functionals compared with experimental values for the lattice constants of graphite. The experimental lattice constants for graphite at ambient pressure: a = 2.464 Å, c = 6.711 Å, and for bcc Potassium: a = 5.247 Å. And whether the vdW functional gives bcc structure as the ground state of potassium at ambient pressure, rather than the fcc structure.

vdW	error of graphite (%)	error of bcc K (%)	bcc K as the ground state
PBE no vdW	δa = 0.08, δ c = 15.4	δa = 0.7	Yes
DFT-D2	δa = -0.08, δ c = -4.2	δa = -1.8	No
DFT-D3	δa = 0.04, δ c = 0.4	δa = -1.6	No
optB88-vdW	δa = 0.2, δ c = -0.01	δa = -0.9	Yes
optPBE-vdW	δa = 0.3, δ c = 2.6	δa = -0.5	Yes
vdWDF2	δa = 0.4, δ c = 5	δa = -1.4	Yes
vdWDF	δa = 0.5, δ c = 6.8	δa = 0.8	Yes

TABLE S2: Lattice parameters of $P4/mmm$-C_4K, $C2/m$-C_3K_4, and $C2/m$-C_2K_3 at 20 GPa.

Phase	Lattice parameters (Å)	Atomic coordinates (fractional)	
C_4K	a = 3.429	C(4l)	0.000 0.700 0.000
$P4/mmm$	c = 4.091	K(1d)	0.500 0.500 0.500
C_3K_4	a = 8.890	C(4i)	0.459 0.000 0.789
	b = 4.695	C(2b)	0.500 0.000 0.000
$C2/m$	c = 7.530	K(4i)	0.747 0.500 0.271
	β = 139.967°	K(4i)	0.062 0.000 0.730
C_2K_3	a = 6.751	C(4i)	0.119 0.500 0.600
	b = 5.941	K(4g)	0.500 0.230 0.000
$C2/m$	c = 4.731	K(2c)	0.500 0.500 0.500
	β = 126.141°		

TABLE S3: The amount of charge tranfer from the intercalated metal atoms to the carbon sheets in C_4K and some typical graphite intercalation compounds.

System	C_4K	C_6Li	C_8Li	C_8Na	C_8K
Charge transfer	0.8e	0.9e	0.8e	0.9e	0.8e

TABLE S4: Calculated values of N_F, V_{ep}, λ, ω_{log} and T_c for C_4K and T graphene at ambient pressure. EPC parameter (λ) and estimated superconducting critical temperature (T_c) with the Coulomb potential (μ^*) of 0.1.

	N_F (states/eV/cell)	V_{ep} (eV)	λ	ω_{log} (cm^{-1})	T_c (K)
C_4K	0.40	2.85	1.14	362.7	30.4
T graphene	0.45	3.49	1.57	175.0	20.8

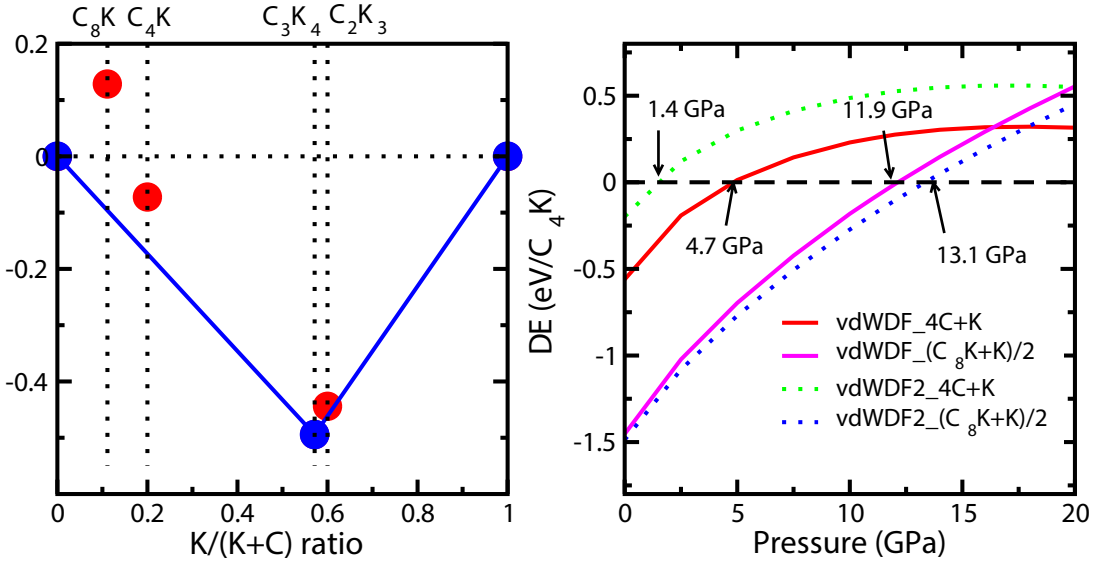

FIG. S1: (a) Convex hulls for C-K system at 20 GPa. The solid tie-lines are drawn by connecting together the globally stable compounds. (b) Calculated enthalpy difference of C + K or C_8K + K relative to C_4K under high pressure, with vdW-DF and vdW-DF2 functionals.

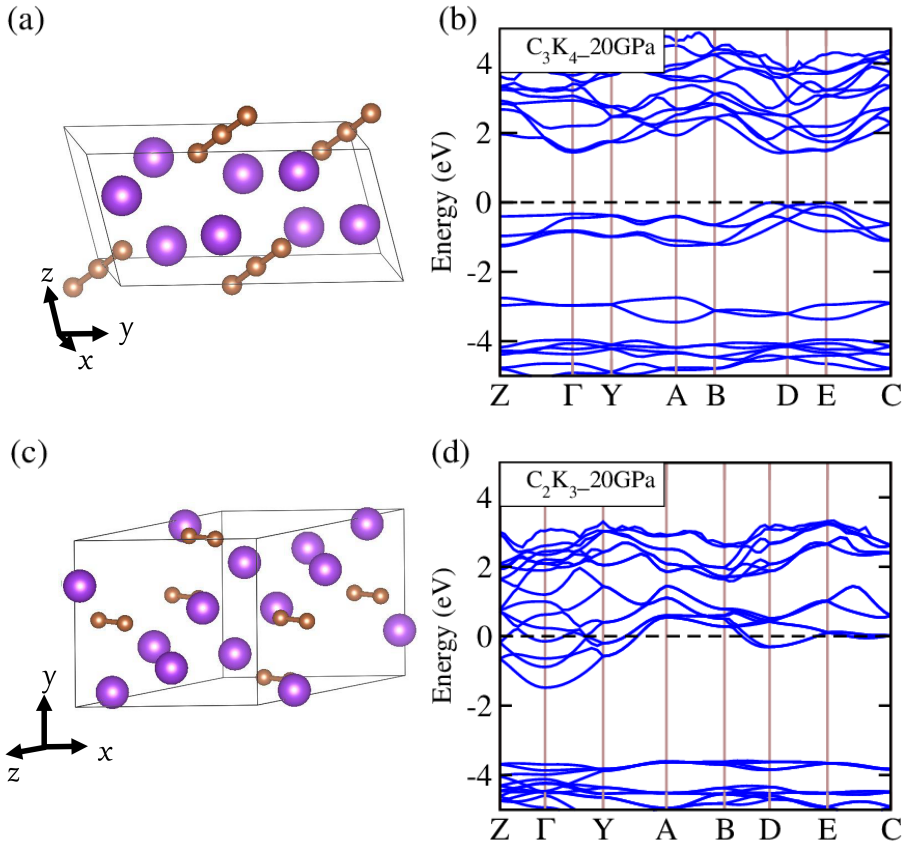

FIG. S2: The crystal structures of (a) C_3K_4 and (c) C_2K_3, yellow and green balls denote C and K atoms, respectively. Calculated electronic structures of (b) C_3K_4 and (d) C_2K_3 at 20 GPa. The Fermi energy is set to zero.

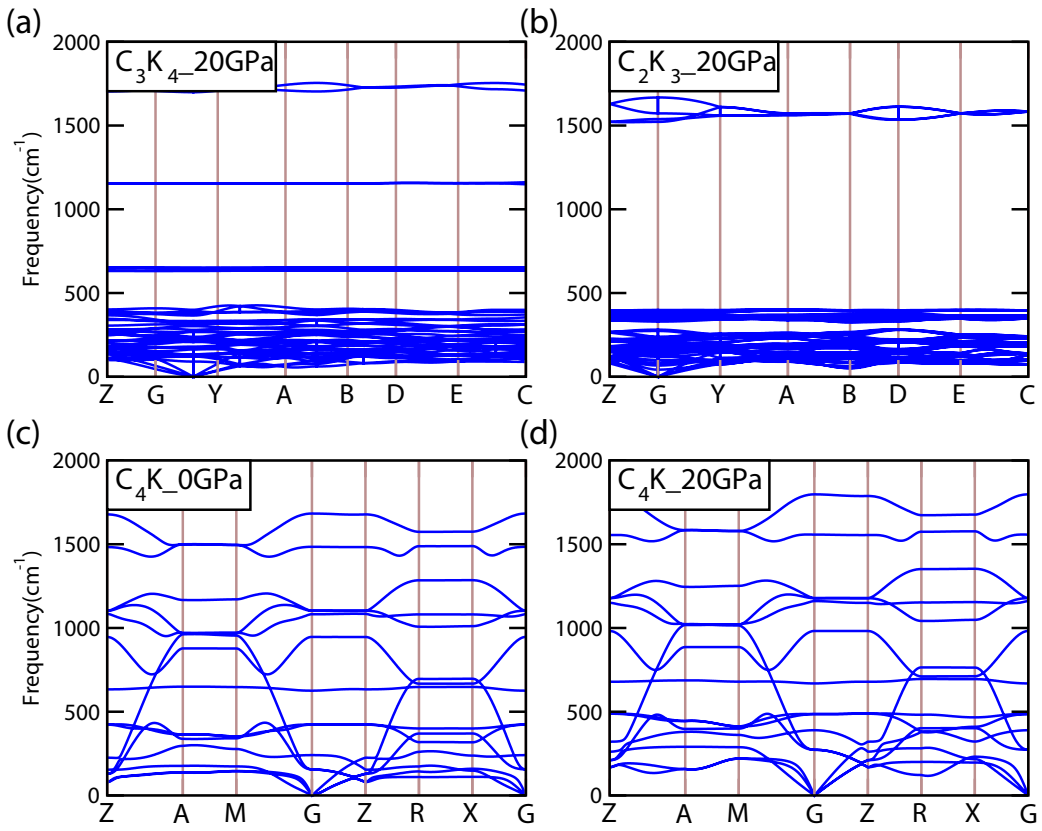

FIG. S3: Calculated phonon spectra for (a) C_3K_4 at 20 GPa, (b) C_2K_3 at 20 GPa and C_4K at (c) 0 GPa, (d) 20 GPa.

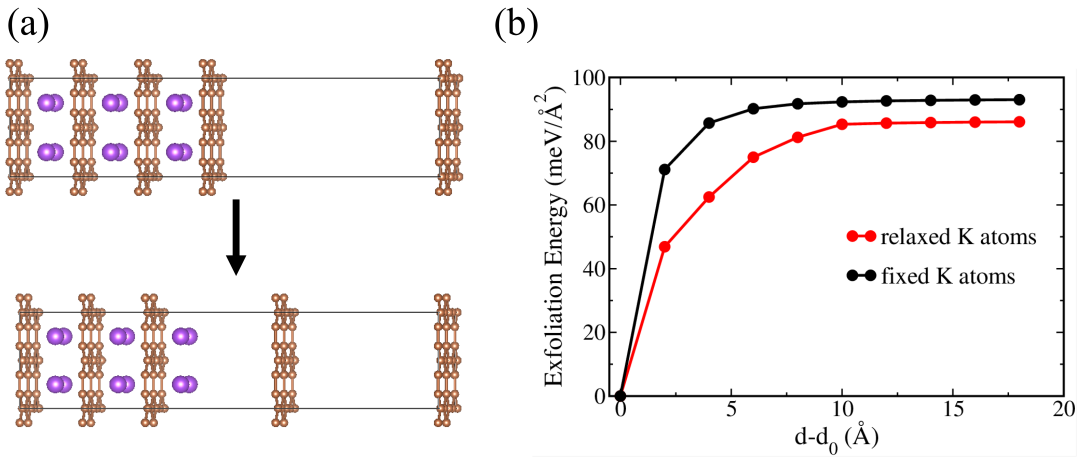

FIG. S4: (a) Schematic of the exfoliating process of T graphene from C_4K, orange and green balls denote C and K atoms, respectively. (b) Calculated exfoliation energies of T graphene from C_4K when only the topmost layer K atoms are relaxed (red line) or all the rest atoms are relaxed (black line).

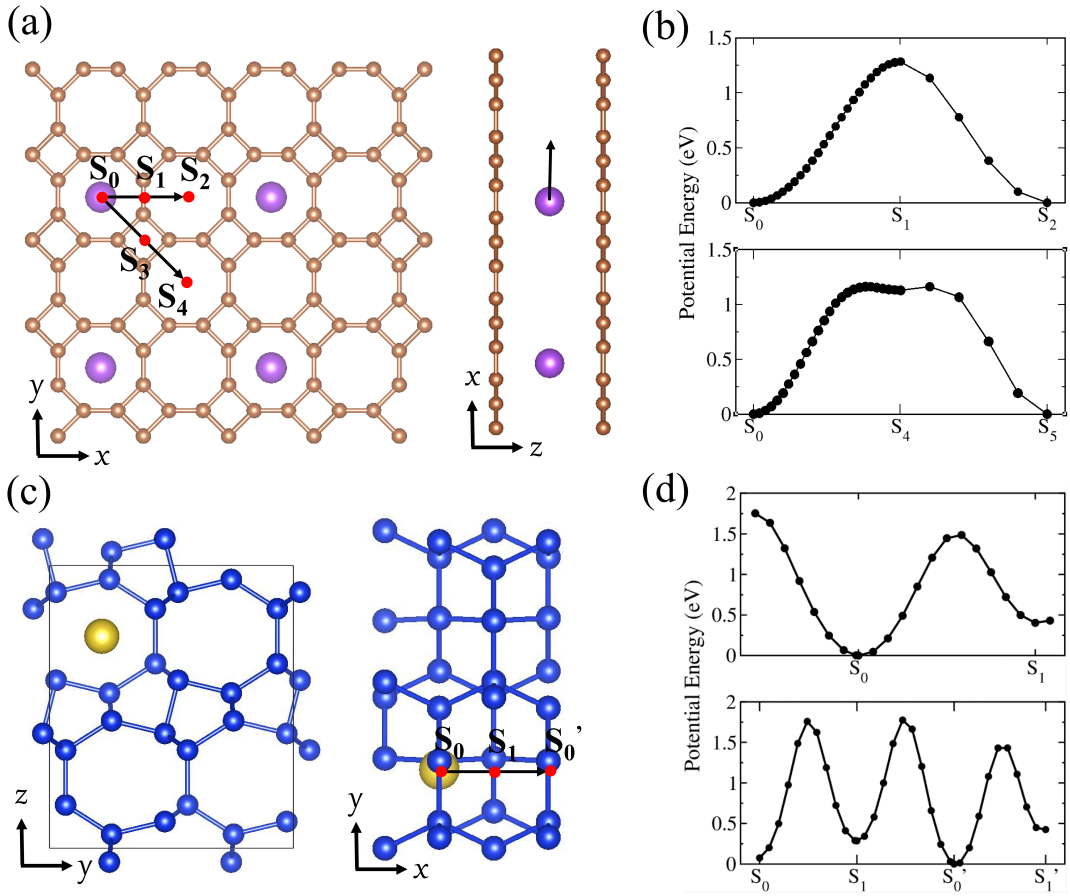

FIG. S5: (a) Diffusion pathways of K atoms in T-graphene layers, K and C atoms are shown with orange and green balls, respectively. (b) Calculated potential energy barriers as the K atom moves through two different paths indicated in (a): from the position S0, S1 to S2, and from the position S0, S3 to S4. (c) Diffusion path way of Na atoms in bulk Si24, yellow and blue balls represent Na and Si atoms, respectively. (d) The calculated potential energy barriers as the Na atom moves through the path indicated in (c): $2 \times 1 \times 1$ (top panel) and $3 \times 1 \times 1$ (bottom panel). The positions labeled by S0, S1, S0' and S1', represent the equilibrium positions of Na atoms in Na4Si24.

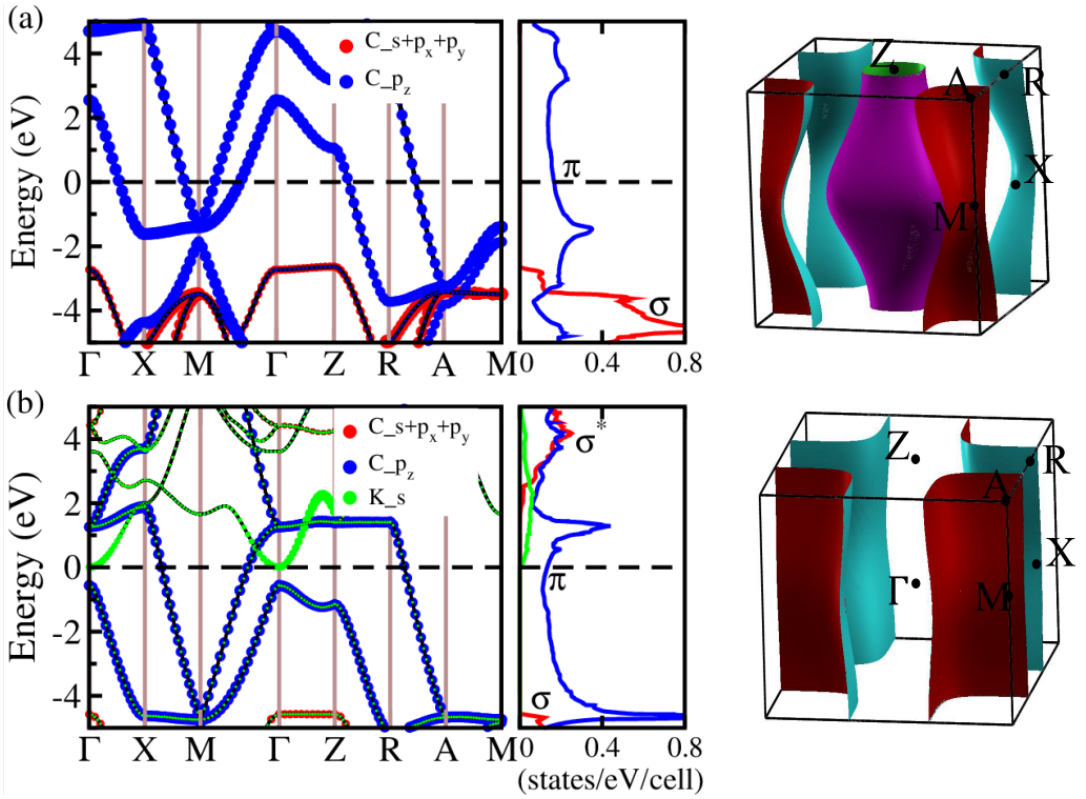

FIG. S6: Calculated electronic structures of C_4K_0 and C_4K at 0 GPa. (a) The orbital-resolved band structures and DOS of C_4K_0 (left panel) and the Fermi surface (right panel). (b) The orbital-resolved band structures and DOS of C_4K (left panel) and the Fermi surface (right panel). The size of the dots in the band structures represents the weights of different orbitals.

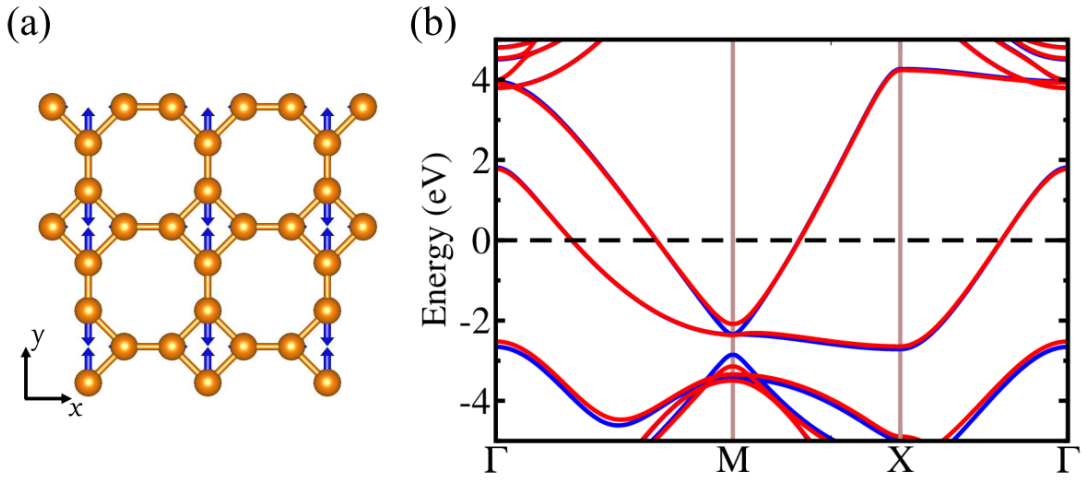

FIG. S7: The Lattice vibration of T graphene. (a) Vibrational patterns for B_{3u} mode. (b) The perturbated (red) and unperturbated (blue) electronic band structures along the B_{3u} mode.

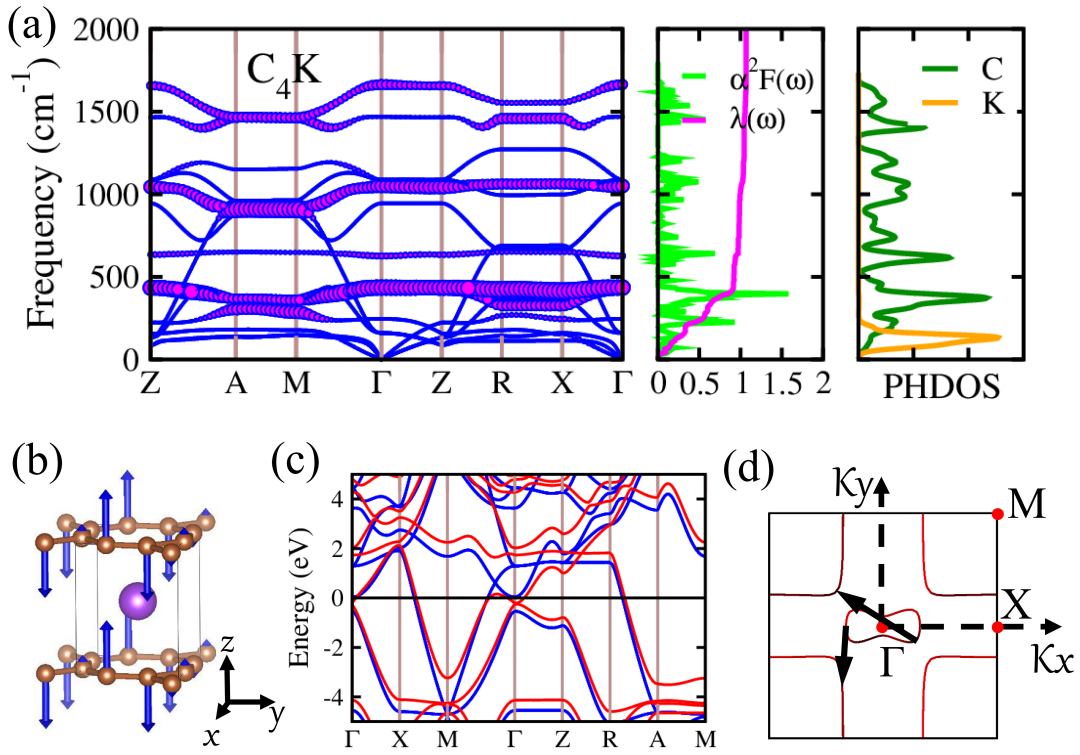

FIG. S8: Electron-phonon structure and Lattice dynamics of C_4K at 0 GPa. (a) Phonon dispersion curves, Eliashberg spectral functions $\alpha^2F(\omega)$ together with the electron-phonon integral $\lambda(\omega)$ and phonon density of states (PHDOS). (b) Vibrational pattern of the E_g mode. (c) The perturbated (red) and unperturbated (blue) electronic band structures along the E_g mode. (d) Fermi surface in the $kz = 0$ plane after perturbation and the arrows point to the nesting vectors.

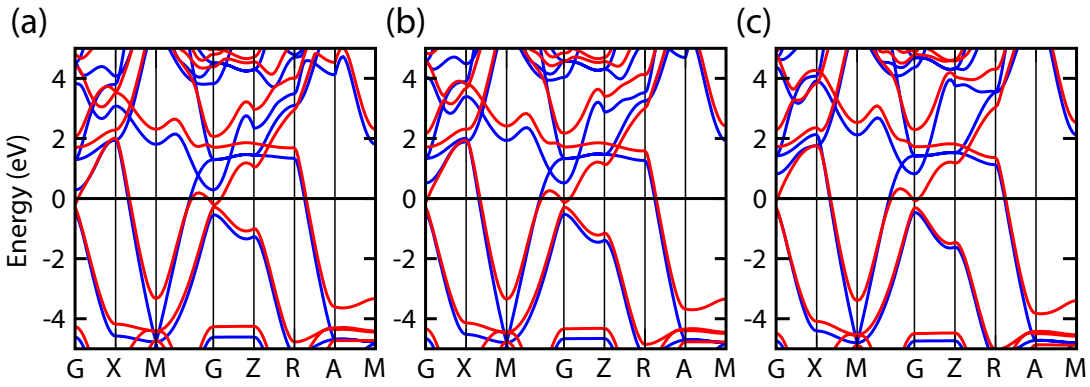

FIG. S9: Calculated electronic structures of C_4K (a) 5 GPa, (b) 10 GPa and (c) 20 GPa. The blue solid lines represent the band before perturbation and the red dashed lines denote the band after perturbation. The Fermi energy is set to zero.

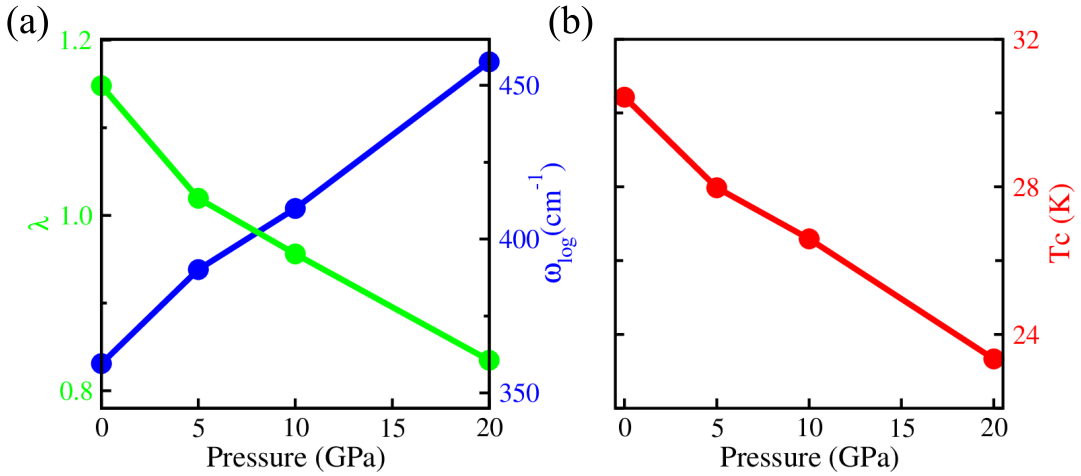

FIG. S10: (a) The coupling parameter λ (green solid line) and logarithmically averaged phonon frequency ω_{log} (blue solid line), and (b) T_c (red solid line) for C_4K as a function of pressure.